Supporting Information

In situ Encapsulation of Co-based nanoparticles into Nitrogen-doped Carbon-Nanotubes modified reduced Graphene Oxide as Air Cathode for High-performance Zn–Air Batteries †

Haocheng Qi, [a,†] *Yingying Feng,* [a,†] *Zhenzhen Chi,* [a,†] *Yuanyuan Cui,* [c] *Minghui Wang,* [a] *Jie Liu,* [a, b] *Ziyang Guo*,* [a] *Lei Wang*,* [a] *and Shouhua Feng* [a]

a State Key Laboratory of Eco-chemical Engineering, College of Chemistry and Molecular Engineering, Qingdao University of Science and Technology, Qingdao 266042, China.

b Guangxi Key Laboratory for Electrochemical Energy Materials, Guangxi University, P. R. China.

c Shimadzu China Co. LTD., Shanghai 200233, China.

---

* Corresponding author. Tel & Fax: 0086-0532-84023409

†These authors contributed equally to this work (Dr. H. Qi, Dr. Y. Feng, and Z. Chi).

E-mail address*: zyguo@qust.edu.cn; inorchemwl@126.com*

Experimental section

***Materials*:** Cobalt nitrate hexahydrate ($CoNO_3$•$6H_2O$, 99 %) was purchased from MACKLIN Reagent. 2-methylimidazole (99 %) was purchased from J&K Scientific Reagent. Cetyltrimethylammonium Bromide (CTAB) was purchased from Tianjin BODI Reagent. Potassium hydroxide (KOH, 90 %) was purchased from Aladdin Reagent. Cobalt chloride hexahydrate ($CoCl_2$•$6H_2O$, 98%) was purchased from Aladdin Reagent. Melamine (99 %) was purchased from Aladdin Reagent. Polyvinyl alcohol (PVA, MW 19500) was purchased from Aladdin Reagent. Polyethylene oxide (PEO, MW 10000) was purchased from Alfa Aesar Reagent. Other chemicals were from Sinopharm Chemical Reagent Corp. All chemicals were used as received without further purification.

Graphene Oxide (GO) preparation: Graphene oxide was obtained according to the Hummer method. Firstly, the aqueous graphene oxide solution was synthesized according to the modified Hummer method. Briefly, the pristine graphite flakes (2 g) was put into the concentrated H_2SO_4 (92 mL) solution containing 2 g $NaNO_3$, which was stirred at 0 °C in a water/ice bath. $KMnO_4$ (12 g) was then gradually added and the mixture was continuously stirred at 0 °C for 90 minutes. Subsequently, the ice bath was removed and the beaker was heated to 35 °C and maintained at this temperature for 2 hours, followed by the slow addition of 92 mL of deionized (DI) water. The temperature of the reaction mixture increased to ~98 °C and the reaction vessel was maintained at this temperature for 1 hour. Then, the suspension was further diluted with 300 mL of additional water and treated with 30 % H_2O_2 until the cessation of gas evolution. After that, a suspension of graphite oxides was obtained. The graphite oxides suspension could settle down and the clear solution at the top was repeatedly removed and replaced with deionized water until the suspension became neutral. Subsequently, the resulting slurry of graphite oxide was subjected to many ultrasonication and centrifugation cycles until no sediment was found at the bottom of the centrifuge tube. Finally, slurry of graphite oxide was freeze-dried overnight to obtain the graphene oxide (GO).

ZIF-8 and ZIF-67 preparation: ZIF-8 nanocubes were prepared using a co-precipitation method. Typically, 82 mL of aqueous solution dissolved by 5.65 g of 2-methylimidazole (2-MeIm) was rapidly mixed with 18 mL of an aqueous solution containing 362 mg of $Zn(NO_3)_2 \cdot 6H_2O$ and 10 mg of cetyltrimethylammonium Bromide (CTAB). Following that, the mixed solution was vigorously stirred for 1 h at room temperature. Finally, the white-colored ZIF-8 precipitate suspension was obtained by centrifugation, washed with a mixed solution of deionized water and ethanol (1 : 1 in volume) for four times, and dried at 60 °C. The fabrication procedure of ZIF-67 composite is similar to that making for ZIF-8 composite but using 354 mg $Co(NO_3)_2 \cdot 6H_2O$ instead of $Zn(NO_3)_2 \cdot 6H_2O$, respectively.

ZIF-8/GO and ZIF-67/GO preparation: In a typical synthesis of ZIF-8/GO, 163 mg of $Zn(NO_3)_2 \cdot 6H_2O$ and 5 mg of CTAB were firstly mixed with 10 mL of 4.5 mg mL^{-1} graphene oxide suspension by stirring for 50 min. Then, 40 mL of deionized water containing 2.825 g of 2-MeIm aqueous solution was added into above solution. After the mixture was stirred at room temperature for 30 min, the resulting precipitates, were centrifuged at 7000 rpm for 15 minutes and washed with ethanol for four times. Finally, the ZIF-8/GO powder was obtained by freeze drying in a freeze dryer with a vacuum at −50 °C for 72 h. The fabrication procedure of ZIF-67/GO composite is similar to that of ZIF-8/GO composite, which just $Co(NO_3)_2 \cdot 6H_2O$ instead of $Zn(NO_3)_2 \cdot 6H_2O$, respectively.

Co/Co_4N@NC/rGO and NC/rGO preparation: Firstly, the above obtained ZIF-8/GO (or ZIF-67/GO) and melamine have been evenly mixed with a mass ratio of 10:1. Then, the as-prepared mixture has further been carbonized at 900 °C for 2 h under Ar gas flowing. After cooling down, the encapsulation of Co/Co_4N nanoparticles in N-doped carbon coated reduced GO (denoted as Co/Co_4N@NC/rGO) or N-doped carbon modified reduced GO (denoted as NC/rGO) can be obtained successfully.

Co/Co_4N@N-CNTs/rGO based flexible cathode preparation: Firstly, 10 wt % KB (Ketjenblack), 80 wt % Co/Co_4N@N-CNTs/rGO and 10 wt % polyvinylidene fluoride binder (PVDF) were intimately mixed in an N-methyl-2-pyrrolidone (NMP) solution, and the resulting slurry was coated on carbon rope. Finally, the coated

electrode was dried for 12 h at 120 °C to remove residual solvent.

Preparation of flexible polymer based Zn–Air Batteries: Firstly, 2 g polyvinyl alcohol (PVA) powder and 0.2 g polyethylene oxide (PEO) powder were dissolved in 10 mL deionized water at 95 °C under magnetic stirring for about 2 h. Then 2 mL of 18 M KOH solution was added and the electrolyte solution was kept stirring at 95 °C for about 40 min. A zinc wire (2 mm in diameter) as the anode was removed in a polyethylene terephthalate (PET) tube template (4 mm in diameter). The tube template was filled with the hydrogel polymer electrolyte solution. After it was kept in a refrigerator at −20 °C for 2 h to crosslink the electrolyte solution, the temperature was increased to 0 °C for 4 h to further enhance the crosslinking degree. Then, the gel polymer coated zinc wire was uniformly wrapped with Co/Co_4N@N-CNTs/rGO based carbon fiber rope. Finally, the above flexible Zn–air battery was sealed into a punched heat shrinkable tube.

ORR and ORR Measurements of catalysts: Electrocatalytic ORR and OER performance were characterized in a three-electrode glass cell. The data were recorded using a Gamry Reference 3000 electrochemical workstation (Gamry instrument co., LTD, America) and Gamry RDE710 rotating electrode (Gamry instrument co., LTD, America). The synthesized Co/Co_4N@N-CNTs/rGO, commercial Pt/C (20 wt% Pt on carbon black) and RuO_2 were thoroughly ground. Thereafter, 4 mg of the material was dispersed in 666 µl of water, 333 µl of ethanol and 120 µl of Nafion by sonicating for 30 minutes to obtain a uniform dispersion. 20 µl of the dispersion was dropped onto the rotating disk electrode and allowed to dry naturally to prepare a working electrode. The reference electrode was Hg/HgO in 1 M KOH solution, and the counter electrode was platinum film. The current density was normalized to the geometrical surface area and the measured potentials vs. Hg/HgO were converted to a reversible hydrogen electrode (RHE) scale according to the Nernst equation ($E_{RHE} = E_{Hg/HgO} + 0.059 \times pH + 0.098$). A flow of O_2 was maintained over the electrolyte (0.1 M KOH) during the recording of electrochemical data in order to ensure the O_2/H_2O equilibrium at 1.23 V vs. RHE. Cyclic voltammograms (CVs) were performed with the scan rate at 5 mV s^{-1}, and working electrodes were

scanned for several times until stabilization before CV data were collected. The linear sweep voltammograms (LSVs) were conducted with the scan rate of 5 mV s^{-1}. The working electrodes were scanned for several times until the signals were stabilized, then LSV data were collected, corrected for the iR contribution within the cell. The Tafel slope was calculated according to Tafel equation as follows:

$$\eta = b \cdot log(j/j_0)$$

where η denotes the overpotential, b denotes the Tafel slope, j denotes the current density, and j_0 denotes the exchange current density. The onset potentials were determined based on the beginning of the linear region in Tafel plots. The overpotential was calculated as follows:

$$\eta = E\ (vs.\ RHE) - 1.23$$

Considering O_2/H_2O equilibrium at 1.23 V *vs.* RHE.

On the basis of RDE data, the electron transfer number per oxygen molecule involved in oxygen reduction can be determined by Koutechy-Levich equation (**ref. S1** and **2**):

$$1/j = 1/j_k + 1/Bw^{1/2} \quad (1)$$

where j_k is the kinetic current and ω is the electrode rotating rate. B is determined from the slope of the Koutechy-Levich (K-L) plots according to the Koutechy-Levich (K-L) equation as given below:

$$B = 0.2nF(D_{O2})2/3\upsilon^{-1/6} C_{O2} \quad (2)$$

where n represents the transferred electron number per oxygen molecule. F is Faraday constant (F = 96485 C mol^{-1}). D_{O2} is the diffusion coefficient of O_2 in 0.1 M KOH (D_{O2} = 1.9 × 10-5 cm^2 s^{-1}). υ is the kinetic viscosity (υ = 0.01 cm^2 s^{-1}). C_{O2} is the bulk concentration of O_2 (C_{O2} = 1.2 ×10^{-6} mol cm^{-3}). The constant 0.2 is adopted when the rotation speed is expressed in rpm.

Characterization instrumentation

XRD measurements were performed on a Bruker D8 Focus power X-ray diffractometer with Cu K_α radiation. SEM investigations were conducted using a JSM-6390 microscope from JEOL. Transmission electron microscopy (TEM) experiments were conducted using a JEOL 2011 microscope (Japan) operated at 200

kV. Specific surface areas were calculated by the Brunaure–Emmert–Teller method. Pore volumes and sizes were estimated from the pore-size distribution curves from the adsorption isotherms using the Barrett–Joyner–Halenda method. X-ray photoelectron spectroscopy (XPS) was conducted with a AXIS Supra by Kratos Analytical Inc. (using monochromatized Al K_{α} radiation (hv = 1486.6 eV, 225 W) as X-ray source with a base pressure of 10−9 torr, A charge neutralizer was used throughout as the samples were mounted such that they were electrically isolated from the sample bar. All spectrums were calibrated by C 1s (284.8 eV)). Electrochemical performance measurements were performed on a Gamry Reference 3000 electrochemical workstation (Gamry instrument co., LTD, America) and Gamry RDE710 rotating electrode (Gamry instrument co., LTD, America).

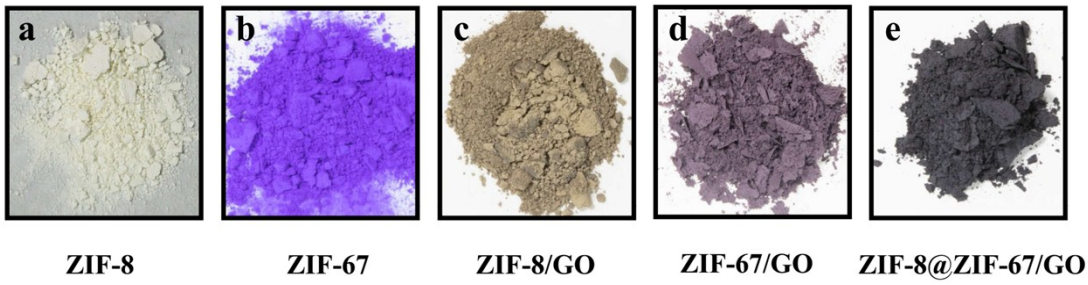

Figure S1 Photograph images of (a) ZIF-8, (b) ZIF-67, (c) ZIF-8/GO, (d) ZIF-67/GO and (e) ZIF-8@ZIF-67/GO

As shown in **Figure S1**, it can be found that ZIF-8@ZIF-67/GO powder is black, which is different from that of ZIF-8 (white), ZIF-67 (purple), ZIF-8/GO (earthy yellow) or ZIF-67/GO (modena).

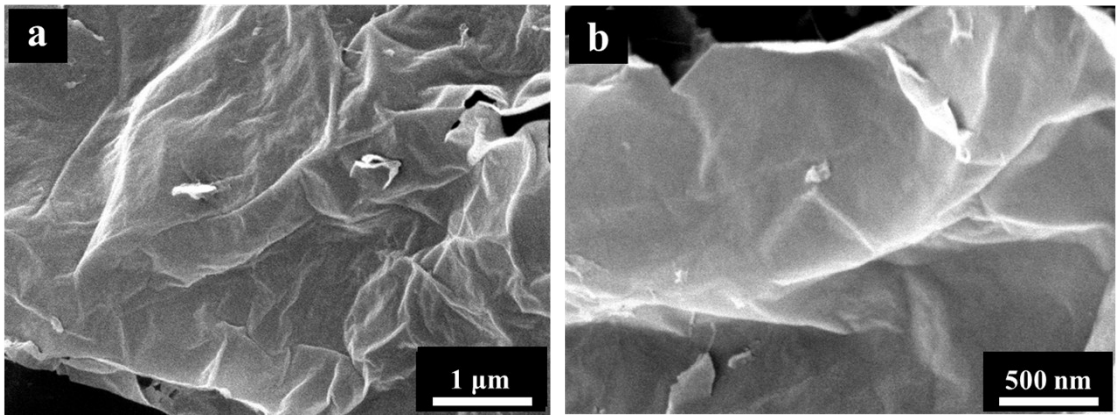

Figure S2 SEM images of GO with different magnifications

As shown in **Figure S2**, GO which has been synthesized by a conventional Hummers method shows the typical sheet structure.

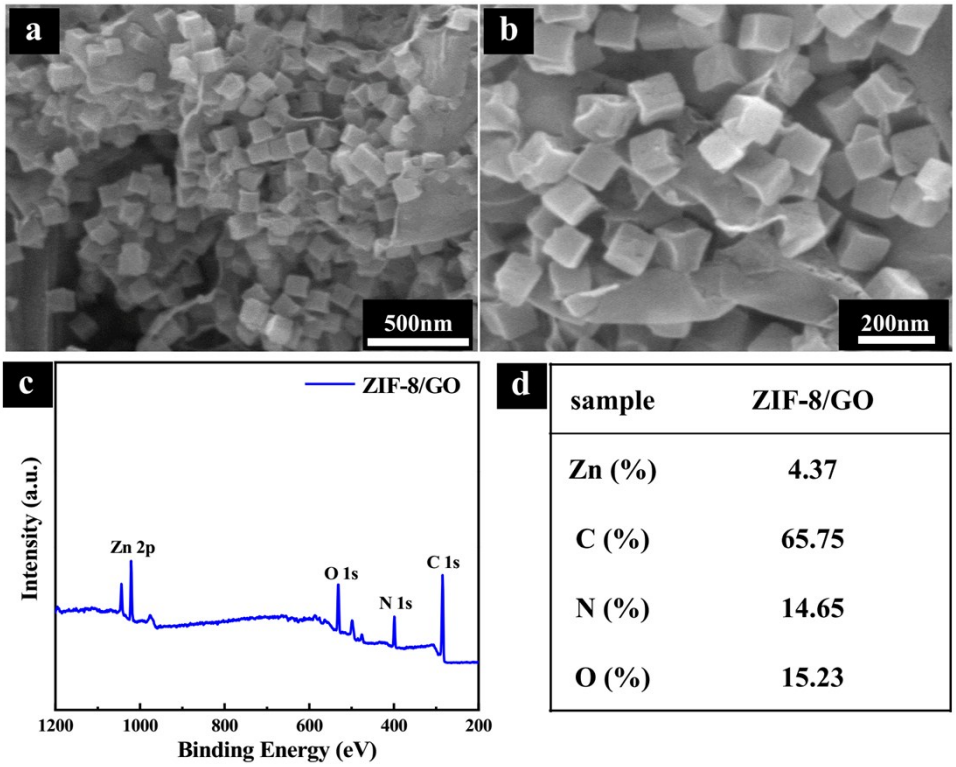

d

sample	ZIF-8/GO
Zn (%)	4.37
C (%)	65.75
N (%)	14.65
O (%)	15.23

Figure S3 (a, b) SEM images of ZIF-8@GO with different magnifications; (c) full XPS spectra and (d) the corresponding surface element contents of ZIF-8@GO.

As shown in the **Figure S3a** and **b**, both sides of GO sheets are uniformly covered with the ZIF-8 nanocubes with average size of ~100 nm. In addition, the full XPS spectra shown in **Figure S3c** exhibit that there are only C, N, and Zn elements in ZIF-8/GO. Moreover, it can be found from **Figure S3d** that the surface content of Zn element in ZIF-8/GO is 4.73%.

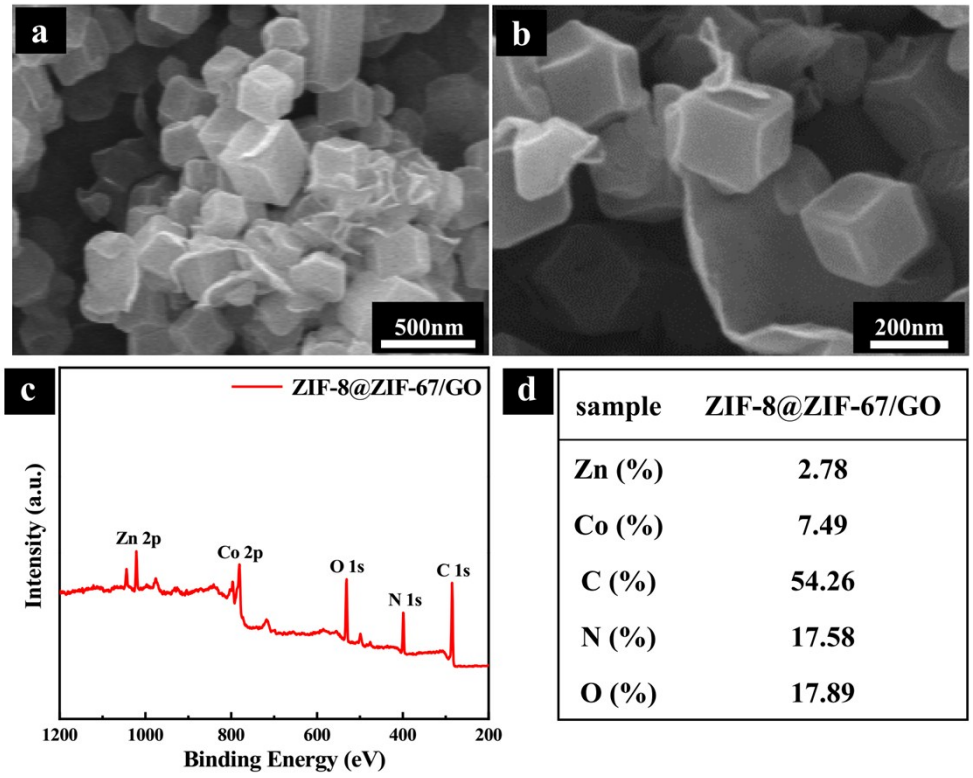

sample	ZIF-8@ZIF-67/GO
Zn (%)	2.78
Co (%)	7.49
C (%)	54.26
N (%)	17.58
O (%)	17.89

Figure S4 (a, b) SEM images of ZIF-8@ZIF-67/GO with different magnifications; (c) full XPS spectra and (d) the corresponding surface element contents of ZIF-8@ZIF-67/GO.

It can be seen from **Figure S4a** and **b** that ZIF-67 epitaxially growing on the surface of ZIF-8 and these ZIFs particles (*i. e.* ZIF-8@ZIF-67) are still anchored on the GO sheet. In addition, ZIF-8@ZIF-67 in ZIF-8@ZIF-67/GO exhibits the polyhedral morphology (**Figure S4**), while the morphology of ZIF-8 in ZIF-8/GO is cubic (**Figure S3**). To further analyze the surface composition of ZIF-8@ZIF-67/GO, XPS technology has also been carried out. The full XPS spectra shown in **Figure S4c** exhibit that there are C, N, Zn and Co elements in ZIF-8@ZIF-67/GO. Moreover, the surface content of Zn element in ZIF-8@ZIF-67/GO is much lower than that in ZIF-8/GO (**Figure S3d** and **4d**). These above results further demonstrate that ZIF-67 is coated on the surface of ZIF-8 nanocubes in ZIF-8@ZIF-67/GO.

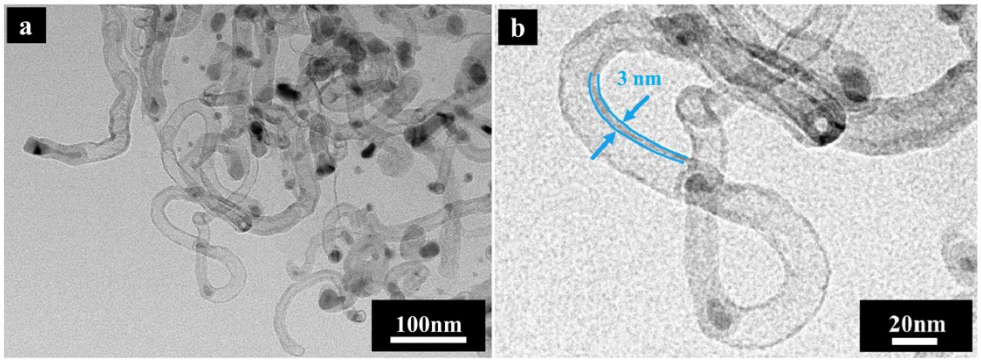

Figure S5 TEM images of the Co/Co_4N@N-CNTs/rGO with different magnifications

As shown in the **Figure S5a**, there are many CNTs in Co/Co_4N@N-CNTs/rGO. In addition, the wall thickness of these CNTs in Co/Co_4N@N-CNTs/rGO is ~3 nm (**Figure S5b**).

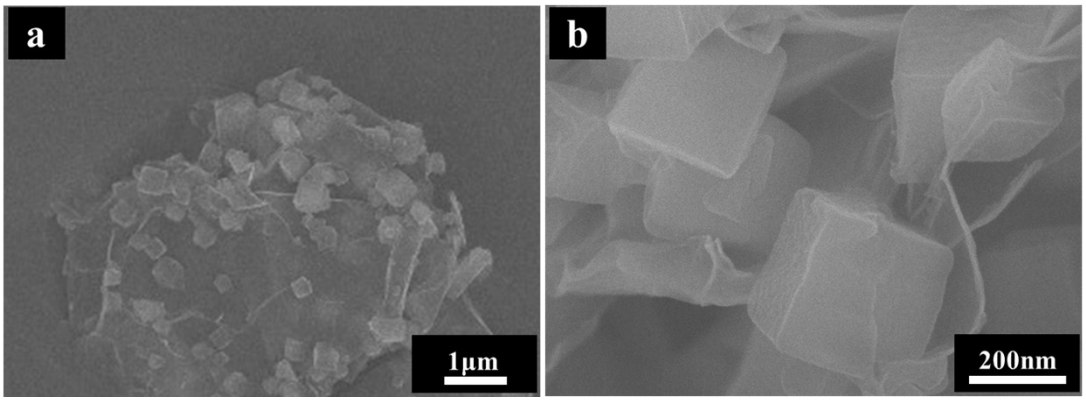

Figure S6 SEM images of ZIF-67/GO with different magnifications

As shown in the F**igure S6**, both sides of GO sheets are tightly embedded with ZIF-67 nanocubes in ZIF-67/GO.

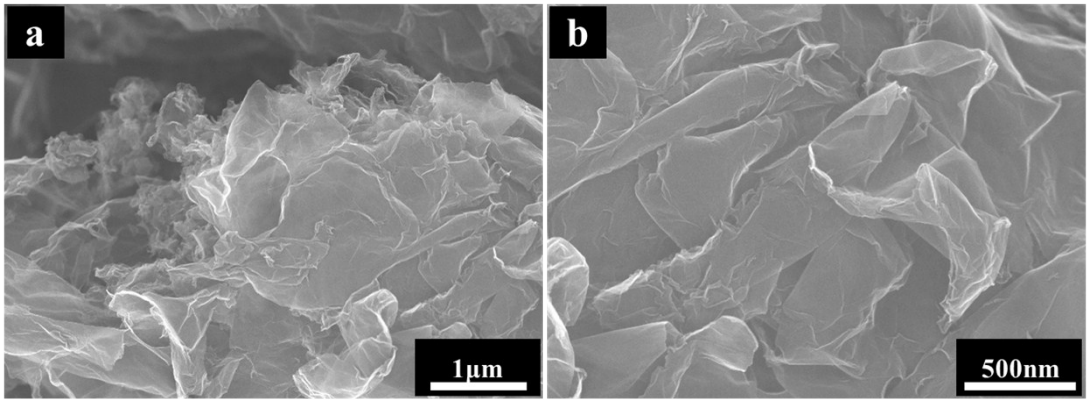

Figure S7 SEM images of NC/rGO with different magnifications

As shown in **Figure S7**, NC/rGO also shows the typical layer structure, which is in agreement with that of GO sheet.

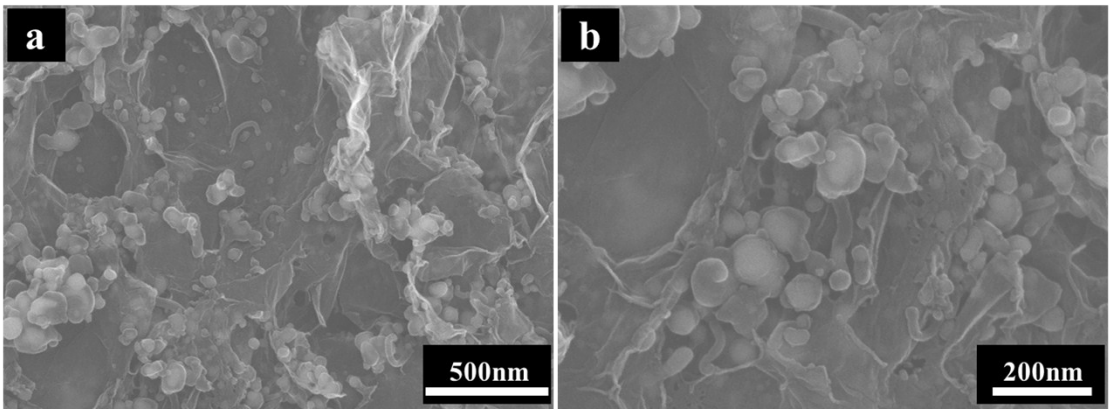

Figure S8 SEM images of Co/Co_4N@NC/rGO with different magnifications

It can be observed from **Figure S8** that there are many Co-based nanoparticles formed on the surface of graphene sheet in Co/Co_4N@NC/rGO. Interestingly, a small amount of CNTs could be also observed in Co/Co_4N@NC/rGO, indicating that Co species played an important role on the formation of CNTs.

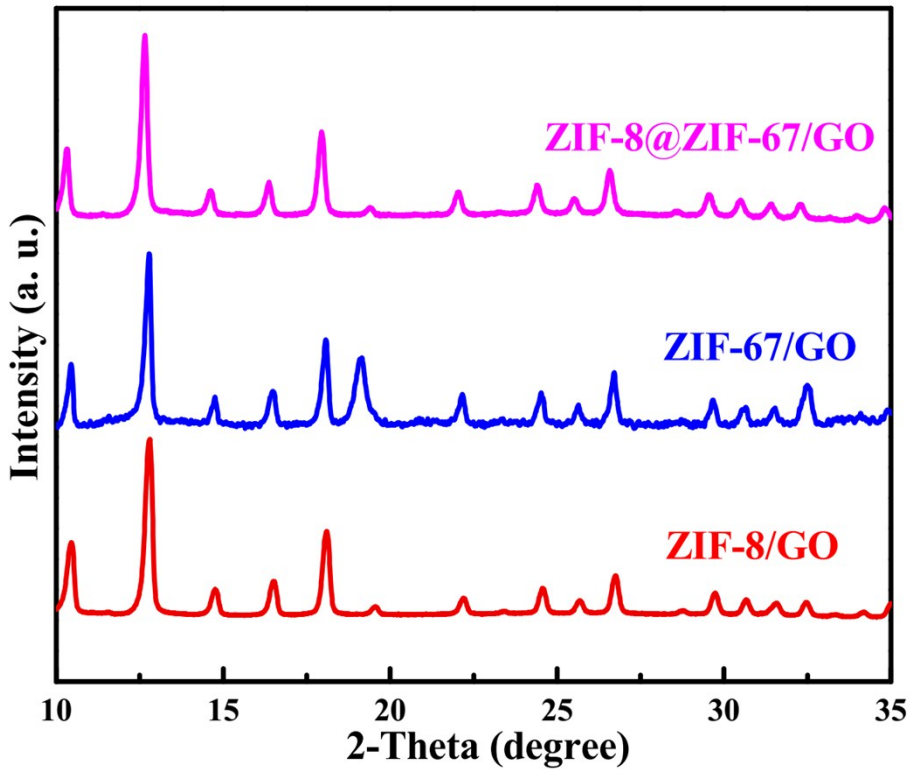

Figure S9 XRD pattern of ZIF-8@GO, ZIF-67@GO and ZIF-8@ZIF-67/GO

The crystal structure of the synthesized materials (*e. g.* ZIF-8@GO, ZIF-67@GO and ZIF-8@ZIF-67/GO) has been identified by XRD analysis (**Figure S9**). As shown in **Figure S9**, XRD patterns for all the above precursors were almost identical to the previously reported XRD pattern of ZIF-8 (**ref. S3**).

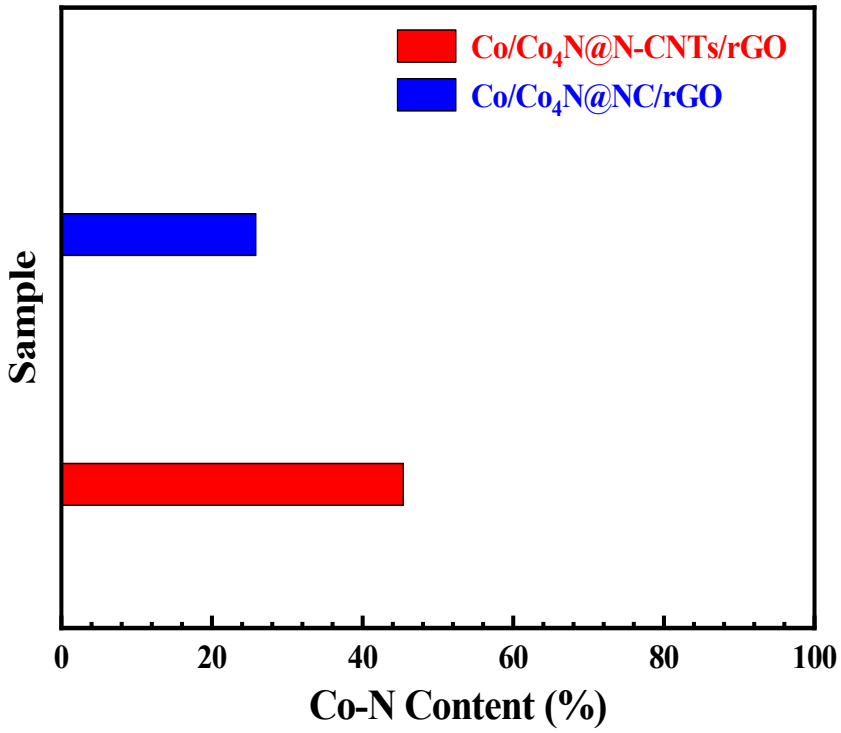

Figure S10 Percentages of Co-N species calculated from Co $2p_{2/3}$ spectra of Co/Co_4N@N-CNTs/rGO and Co/Co_4N@NC/rGO

As shown in the **Figure S10**, the Co-N content in Co/Co_4N@N-CNTs/rGO is 45.4 %, which is higher than that of Co/Co_4N@NC/rGO (25.8 %). Co-N species have been demonstrated to enhance the OER activity. This result suggests the superior catalytic activity of Co/Co_4N@N-CNTs/rGO towards OER.

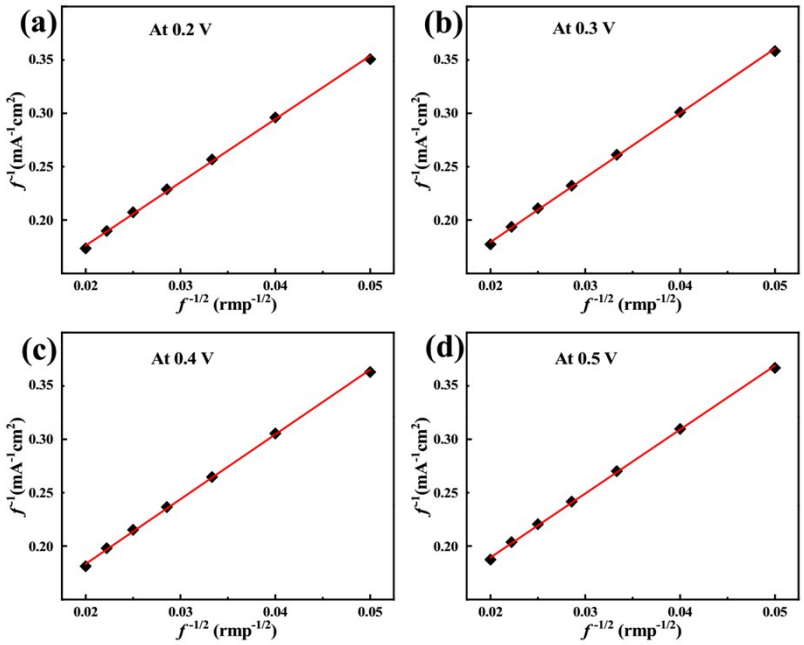

Figure S11 The K-L plots of Co/Co_4N@N-CNTs/rGO at various potentials: (a) 0.2 V, (b) 0.3 V, (c) 0.4 V and (d) 0.5V.

As shown in **Figure S11**, all the Koutecky–Levich (K–L) plots exhibit the excllent linearity, suggesting a first-order reaction kinetics towards the concentration of dissolved O_2 for Co/Co_4N@N-CNTs/rGO during the ORR process at all the potentials. From the K–L equation, the electron transfer of Co/Co_4N@N-CNTs/rGO was calculated to be approximately 4.0 in the potential range of 0.2-0.5 V, demostrating the ORR over Co/Co_4N@N-CNTs/rGO proceeds via a typical four-electron pathway.

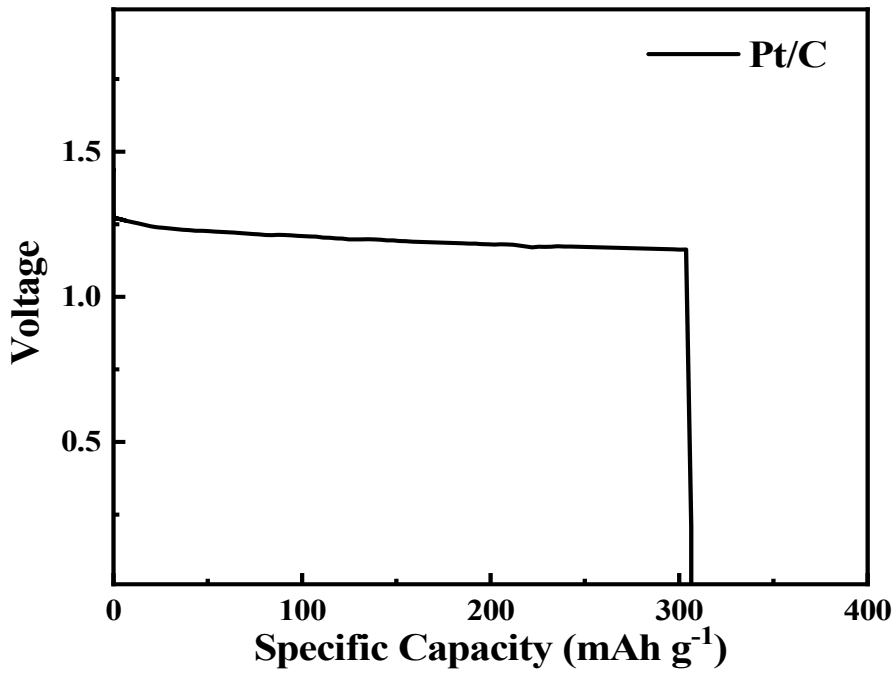

Figure S12 Long-time discharge curves of the primary Zn–air batteries with Pt/C cathodes at a current density of 5 mA cm^{-2}

As shown in the **Figure S12**, the Pt/C-based Zn–air battery exhibits a low specific capacity of 307 mAh g_{Zn}^{-1} at a current density of 5 mA cm^{-2}, which is lower than that of Co/Co_4N@N-CNTs/rGO cathode (**Figure 4c**), suggesting the excellent ORR activity of Co/Co_4N@N-CNTs/rGO.

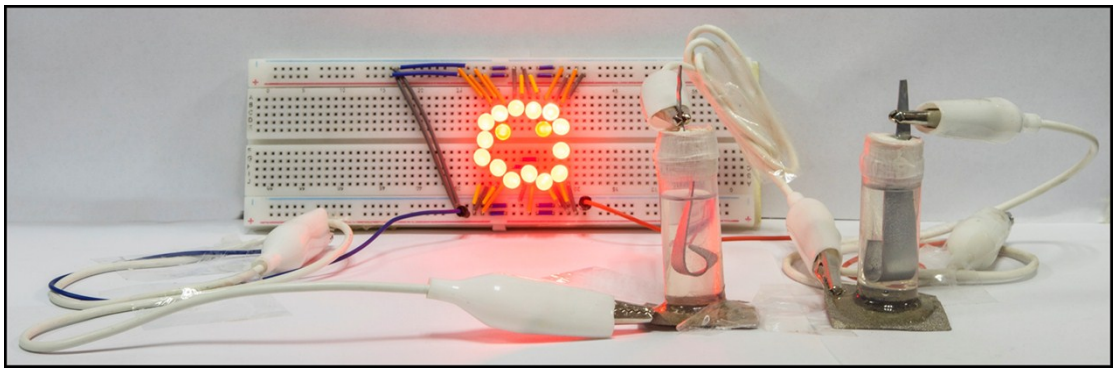

Figure S13 Photographs of 16 LEDs driven by two Co/Co_4N@N-CNTs/rGO-based conventional Zn–air batteries

As shown in **Figure S13**, two Zn–air batteries with Co/Co_4N@N-CNTs/rGO cathode in series could make 16 LEDs light.

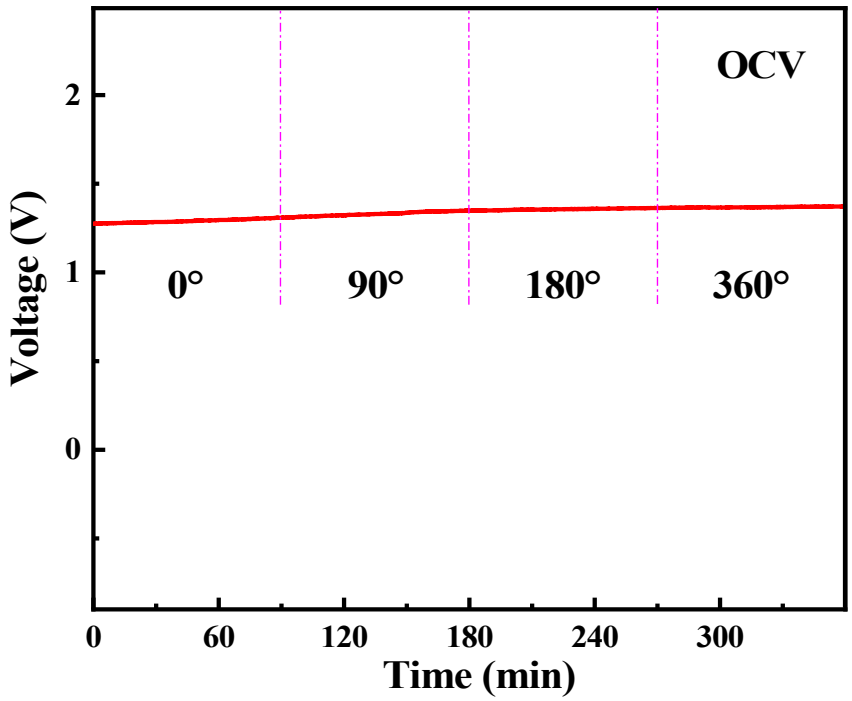

Figure S14 Open-circuit voltage curve of the flexible Zn–air battery using Co/Co_4N@N-CNTs/rGO cathode at different bending conditions

As shown in **Figure S14**, the flexible Co/Co_4N@N-CNTs/rGO-based Zn–air battery displays the high and stable open-circuit voltage of ~1.33 V at different angles of 0°, 90°,180° and 360°, respectively.

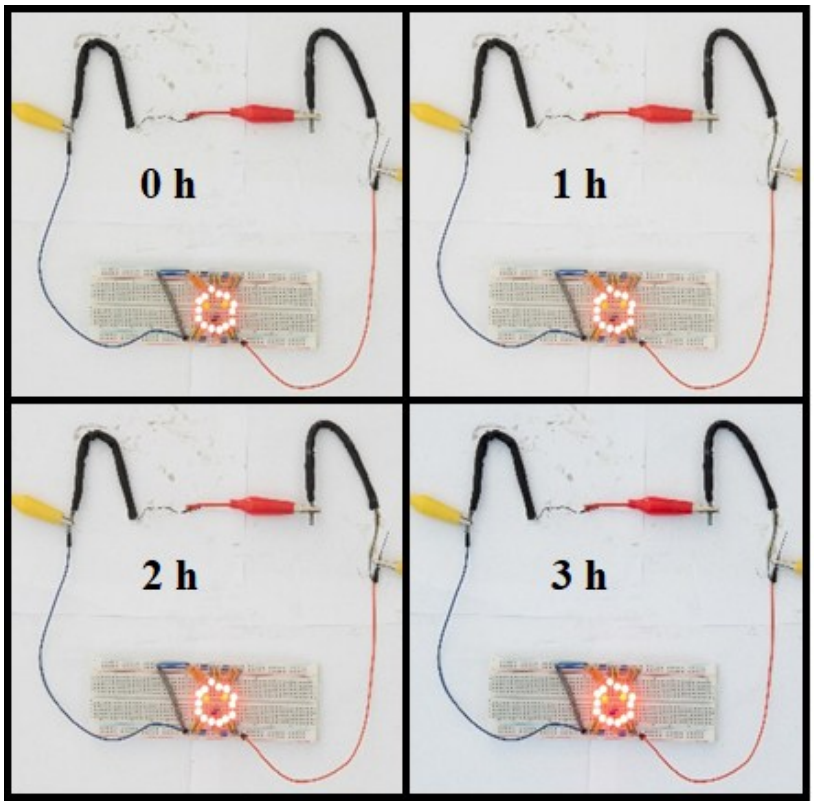

Figure S15 Photographs of 16 LEDs driven by two flexible Zn–air batteries with Co/Co_4N@N-CNTs/rGO cathodes during different times.

As shown in **Figure S15**, two flexible Co/Co_4N@N-CNTs/rGO-based Zn–air batteries can continually light up 16 red light emitting diodes (LED) for 3h, implying a practical potential of the flexible Zn–air batteries using Co/Co_4N@N-CNTs/rGO cathodes.

Table S1 Summary of specific capacity under 5 mA cm^{-2} of various catalysts

Catalysts	Specific Capacity (mAh g^{-1}_{Zn}) Under 5mA cm^{-2}	Reference
Zn-$NiCo_2S_4$HB	**688**	**Ref. S4**
Ni-Mo/rGO	**758**	**Ref. S5**
CoIn_2S_4/S-rGO	**745**	**Ref. S6**
CuS/NiS_2	**775**	**Ref. S7**
N,S-CC	**715**	**Ref. S8**
Au-NWs/Ni_6MnO_8	**760**	**Ref. S9**
Co@Co_3O_4@NC-900	**685**	**Ref. S10**
Co/Co_4N@N-CNTs/rGO	**783**	**This work**

As shown in **Table S1**, the Zn–air battery with Co/Co_4N@N-CNTs/rGO cathode delivered a high specific capacity of 783 mAh g_{Zn}^{-1}, which is obviously higher than most of the recently reported catalysts (**ref. S4-10**).

Table S2 Summary of various electrocatalysts for the rechargeable Zn–air batteries

Catalysts	Cycle number	Total Cycle Time (hour)	Reference
Fe-N_4 SAs/NPC	108@2 mA cm^{-2}	36	Ref. S11
CoS_x/Co-NC-800	450@5 mA cm^{-2}	90	Ref. S12
ZIF-L-D-Co_3O_4/CC	2304@5 mA cm^{-2}	384	Ref. S13
Fe-N-C PCSs	300@10 mA cm^{-2}	100	Ref. S14
Co_3C-NB	900@10 mA cm^{-2}	180	Ref. S15
Au-NWs/Ni_6MnO_8	240@10 mA cm^{-2}	80	Ref. S9
$NiCo_2O_4$@N-OCNT	190@10 mA cm^{-2}	42	Ref. S16
$Coln_2S_4$/S-rGO	150@10 mA cm^{-2}	50	Ref. S6
CoFe/N-CNT	1600@10 mA cm^{-2}	267	Ref. S17
FeN_x/C-700-20	504@5 mA cm^{-2}	84	Ref. S18
N, P/CoS_2@TiO_2	225@10 mA cm^{-2}	150	Ref. S19
Co/Co_4N@N-CNTs/rGO	220@@5 mA cm^{-2}	440	This work

It can be observed from **Table S2** that the Co/Co_4N@N-CNTs/rGO-based Zn–air cell can be stably operated over more than 440 h at a current density of 5 mA cm^{-2} (2 h per cycle), which is obviously higher than most of the state-of-the-art catalysts (**ref. S6, 9 and 11-19**).

Reference

ref. S1: Y. Guo, P. Yuan, J. Zhang, H. Xia, F. Cheng, M. Zhou, J. Li, Y. Qiao, S. Mu and Q. Xu, Co_2P–CoN Double Active Centers Confined in N-Doped Carbon Nanotube: Heterostructural Engineering for Trifunctional Catalysis toward HER, ORR, OER, and Zn–Air Batteries Driven Water Splitting, *Adv. Funct. Mater.*, **2018**, 28, 1805641.

ref. S2: F. Meng, H. Zhong, D. Bao, J. Yan and X. Zhang, In Situ Coupling of Strung Co_4N and Intertwined N–C Fibers toward Free-Standing Bifunctional Cathode for Robust, Efficient, and Flexible Zn–Air Batteries, *J. Am. Chem. Soc.*, **2016**, 138, 10226-10231.

ref. S3: Z. L. Chen, R. B. Wu, Y. Liu, Y. Ha, Y. H. Guo, D. L. Sun, M. Liu and F. Fang, Ultrafne Co Nanoparticles Encapsulated in Carbon Nanotubes-Grafted Graphene Sheets as Advanced Electrocatalysts for the Hydrogen Evolution Reaction, *Adv. Mater.*, **2018**, 30, 1802011.

ref. S4: X. X. Wang, X. X. Xu, J. Cheng and Q. Wang, Combination of Zn–$NiCo_2S_4$ and Zn–Air Batteries at the Cell Level: A Hybrid Battery Makes the Best of Both Worlds, *ACS. Sustain. Chem. Eng.*, **2019**, 7, 12331-12339.

ref. S5: G. Fu, X. Yan, Y. Chen, L. Xu, D. Sun, J. M. Lee and Y. Tang, Boosting Bifunctional Oxygen Electrocatalysis with 3D Graphene Aerogel-Supported Ni/MnO Particles, *Adv. Mater.,* **2018**, 30, 1704609.

ref. S6: G. Fu, J. Wang, Y. Chen, Y. Liu, Y. Tang, J. B. Goodenough and J. M. Lee, Exploring Indium-Based Ternary Thiospinel as Conceivable High-Potential Air-Cathode for Rechargeable Zn-Air Batteries, *Adv. Energy Mater.*, **2018**, 8, 1802263.

ref. S7: L. An, Y. X. Li, M. C. Luo, J. Yin, Y. Q. Zhao, C. L. Xu, F. Y. Cheng, Y. Yang, P. X. Xi and S. J. Guo, Atomic-Level Coupled Interfaces and Lattice Distortion on CuS/NiS_2 Nanocrystals Boost Oxygen Catalysis for Flexible

Zn-Air Batteries, *Adv. Funct. Mater.,* **2017**, 27, 1703779

ref. S8: Z. Zhao, Z. Yuan, Z. Fang, J. Jian, J. Li, M. Yang, C. Mo, Y. Zhang, X. Hu, P. Li, S. Wang, W. Hong, Z. Zheng, G. Ouyang, X. Chen and D. Yu, In Situ Activating Strategy to Significantly Boost Oxygen Electrocatalysis of Commercial Carbon Cloth for Flexible and Rechargeable Zn-Air Batteries, *Adv. Sci.*, **2018**, 5, 1800760.

ref. S9: G. Fu, X. Jiang, Y. Chen, L. Xu, D. Sun, J. M. Lee and Y. Tang, Robust bifunctional oxygen electrocatalyst with a "rigid and flexible" structure for air-cathodes, *NPG Asia Mater.*, **2018**, 10, 618-629.

ref. S10: Z. Y. Guo, F. M. Wang, Y. Xia, J. L. Li, A. G. Tamirat, Y. R. Liu, L. Wang, Y. G. Wang and Y. Y. Xia, In situ encapsulation of core–shell-structured Co@Co_3O_4 into nitrogen-doped carbon polyhedra as a bifunctional catalyst for rechargeable Zn–air batteries. *J. Mater. Chem. A*, **2018**, 6, 1443-1453.

ref. S11: Y. Pan, S. Liu, K. Sun, X. Chen, B. Wang, K. Wu, X. Cao, W. C. Cheong, R. Shen and A. Han, A Bimetallic Zn/Fe Polyphthalocyanine-Derived Single-Atom Fe-N_4 Catalytic Site: A Superior Trifunctional Catalyst for Overall Water Splitting and Zn–Air Batteries, *Angew. Chem. Int. Ed.,* **2018**, 57, 8614.

ref. S12: Q. Lu, J. Yu, X. Zou, K. Liao, P. Tan, W. Zhou, M. Ni and Z. Shao, Self-Catalyzed Growth of Co, N-Codoped CNTs on Carbon-Encased CoS_x Surface: A Noble-Metal-Free Bifunctional Oxygen Electrocatalyst for Flexible Solid Zn–Air Batteries, *Adv. Funct. Mater.,* **2019**, 1904481.

ref. S13: Y. Zhong, Z. Pan, X. Wang, J. Yang, Y. Qiu, S. Xu, Y. Lu, Q. Huang and W. Li, Hierarchical Co_3O_4 Nano-Micro Arrays Featuring Superior Activity as Cathode in a Flexible and Rechargeable Zinc-Air Battery, *Adv. Sci.*, **2019**, 6, 1802243.

ref. S14: J. -T. Ren and Z.-Y. Yuan, A universal route to N-coordinated metals anchored on porous carbon nanosheets for highly efficient oxygen electrochemistry, *J. Mater. Chem. A*, **2019**, 7, 13591-13601.

ref. S15: X. Ma, K. Li, X. Zhang, B. Wei, H. Yang, L. Liu, M. Zhang, X. Zhang and

Y. Chen, The surface engineering of cobalt carbide spheres through N, B co-doping achieved by room-temperature in situ anchoring effects for active and durable multifunctional electrocatalysts, *J. Mater. Chem. A*, **2019**, 7, 14904-14915.

ref. S16: S. Zeng, X. Tong, S. Zhou, B. Lv, J. Qiao, Y. Song, M. Chen, J. Di and Q. Li, All-in-One Bifunctional Oxygen Electrode Films for Flexible Zn-Air Batteries, *Small*, **2018**, 14, e1803409.

ref. S17: X. Liu, L. Wang, P. Yu, C. Tian, F. Sun, J. Ma, W. Li and H. Fu, A Stable Bifunctional Catalyst for Rechargeable Zinc-Air Batteries: Iron-Cobalt Nanoparticles Embedded in a Nitrogen-Doped 3D Carbon Matrix, *Angew. Chem. Int. Ed*., **2018**, 57, 16166-16170.

ref. S18: S. Han, X. Hu, J. Wang, X. Fang and Y. Zhu, Novel Route to Fe-Based Cathode as an Efficient Bifunctional Catalysts for Rechargeable Zn-Air Battery, *Adv. Energy Mater.*, **2018**, 8, 1800955.

ref. S19: L. Guo, J. Deng, G. Wang, Y. Hao, K. Bi, X. Wang and Y. Yang, N, P-doped CoS_2 Embedded in TiO_2 Nanoporous Films for Zn-Air Batteries, *Adv. Funct. Mater.*, **2018**, 28, 1804540.